University of Baghdad
College of Engineering
JE
JOURNAL OF ENGINEERING

Journal of Engineering

journal homepage: www.joe.uobaghdad.edu.iq

Volume 30 Number 1 January 2024

Improving the Direction of Arrival Estimation Using the Parasitic Subspace Generated by Active-Parasitic Antenna (APA) Arrays

Rabah Abduljabbar Jasem

Technical Institute of Al-Dour, Northern Technical University, Salah Al-Din, Iraq
rabah.aj@ntu.edu.iq, rabah_alobaidi5@yahoo.com

ABSTRACT

The improvement in Direction of Arrival (DOA) estimation when the received signals impinge on Active-Parasitic Antenna (APA) arrays will be studied in this work. An APA array consists of several active antennas; others are parasitic antennas. The responses to the received signals are measured at the loaded terminals of the active element. The terminals of the parasitic element are shorted. The effect of the received signals on the parasites, i.e., the induced short-circuit current, is mutually coupled to the active elements. Eigen decomposition of the covariance matrix of the measurements of the APA array generates a third subspace in addition to the traditional signal and noise subspaces generated by the all-active antenna receiving array. This additional subspace, the parasitic subspace, is accompanied by very small eigenvalues (approaching zero). Hence, a complete orthogonality between this subspace and the column space of the steering matrix of the array can be obtained. As a result, better resolution in estimating the DOA can be achieved. Several simulations in conjunction with the MUSIC algorithm, which have been conducted in this work, depict that the APA array outperforms the all-active antenna array as a direction finder, regardless of the size of the array, the number of active elements, or the number of measurement snapshots. Furthermore, super-resolution DOA estimation can be achieved when a subset of the parasitic subspace is used as if the measurement were noiseless. Also, the APA array contributes to very small RMSE values over a wide range of S/N of the received signals.

Keywords: All-active antenna arrays, APA array, DOA estimation, MUSIC algorithm, Mutual coupling, RMSE criterion.

*Corresponding author
Peer review under the responsibility of University of Baghdad.
https://doi.org/10.31026/j.eng.2024.01.11

Article received: 20/05/2023
Article accepted: 25/12/2023
Article published: 01/01/2024

تحسين تخمين اتجاه وصول الموجات الكهرومغناطيسية باستخدام الفضاء الجزئي الطفيلي والمتولد من قياسات مصفوفات المتالفة من هوائيات فعالة وطفيلية

رباح عبد الجبار جاسم

الجامعة التقنية الشمالية – المعهد التقني في الدور، صلاح الدين، العراق

الخلاصة

في هذا البحث سيتم دراسة امكانية تحسين تخمين اتجاه وصول الموجات الكهرومغناطيسية والمستلمة من قبل مصفوفة الهوائيات والمسماه مصفوفة الهوائيات الفعالة والطفيلية. الهوائيات الفعالة هي الهوائيات التي تتولد عبر الحمل المربوط على طرفيها فولتية تمثل استجابة الهوائي للاشارة المستلمة اما الهوائي الطفيلي فيكون طرفيه مربوطين عبر دائرة قصر. استجابة الهوائيات الطفيلية (كتيارات دائرة قصر متولدة فيهم) ينتقل للهوائيات الفعالة عبر خاصية الاقتران المتبادل. التقسيم الايكني لمصفوفة التغاير لقياسات هذه المصفوفات ينتج فضاء جزئي وبقيم ايكن قليلة جدا وبالتالي فان هذا الفضاء الجزئي يكون متعامد بصورة تامة على فضاء المتجهات العمودية لمصفوفة التوجيه. وعليه فان عملية تخمين اتجاهات وصول الاشارات المستلمة بواسطة هذه المصفوفات احسن بكثير من مصفوفات الهوائيات الفعالة فقط. النتائج المستحصلة من هذا البحث تبين بان مصفوفة الهوائيات الفعالة الطفيلية وباستخدام خوارزمية ميوزك تتفوق في تخمين اتجاهات الوصول للاشارات المستلمة على مصفوفات الهوائيات الفعالة فقط بغض النظر عن حجم المصفوفة او عدد الهوائيات الفعالة. بالاضافة الى هذه الفوائد فان استخدام هذه المصفوفات ينتج فارق صغير جدا بين اتجاه الوصول التخميني والحقيقي عبر حساب مقياس الجذر التربيعي لمعدل مربع الخطأ.

الكلمات المفتاحية: مصفوفات الهوائيات الفعالة فقط, مصفوفات الهوائيات الفعالة الطفيلية, الاقتران المتبادل, اتجاه الوصول, خوارزمية ميوزك, مقياس الجذر التربيعي لمعدل مربع الخطأ.

1. INTRODUCTION

Estimating the direction of arrival (DOA) is an active topic in the telecommunications and signal-processing fields. Determining the location and tracking a target or the user, for example, in mobile communications, depends on precise DOA estimates of that target **(Van Trees, 2002; Tuncer and Friedlander, 2009; Chen et al., 2010; Chandran, 2005**). Also, several applications, including radar, sonar, wireless communications, etc., rely on accurate DOA estimation. Recently, DOA estimation has effectively tracked patient's conditions **(Wan et al., 2016).** Targeting underwater objects requires sophisticated DOA estimation methods like those presented in **(Jing et al., 2018; Hamid et al., 2023)**. In **(Chen, 2019)**, DOA estimation is used to indicate the degradation of the insulation material in power transformers.

Antenna arrays can be used for this purpose. Under certain conditions, the measurements of antenna arrays can be used to estimate the DOA of received signals by analyzing these measurements (the array's response to the received signals) and processing the results along with DOA estimation algorithms such as ESPRIT and MUSIC. The spectral decomposition of the covariance matrix of these measurements is used to determine two

orthogonal subspaces: signal and noise subspaces **(Schmidt, 1986; Roy and Kailath, 1989; Eranti and Barkana, 2022)**. The MUSIC algorithm searches the peaks when a subset of the search vectors, which correspond to the DOAs, is orthogonal to the estimated noise subspace **(Schmidt, 1986).**

Using smart antenna arrays may strengthen and improve the performance of high-resolution DOA estimation algorithms **(Lan et al., 2022),** perhaps outperforming traditional antenna arrays. When adopting smart antenna arrays, multi-path and co-channel interference are significantly decreased. Also, knowledge of DOAs helps an antenna array's beam take on the required shape **(El Zooghby, 2005; Zhao et al., 2020).** On the other hand, working on beam rather than element space enhances DOA estimation performance when the received signals are coherent and reduce computational complexity **(Ferreira et al., 2008; Sun and Yang, 2004)**. Because of the versatility and amenities that smart antenna arrays offer for the newest generations of mobile communications, demand for them has expanded quickly **(El Zooghby, 2005)**. The Switched Parasitic Antenna (SPA) array is one of these smart antennas in which the antennas are quickly and easily switched between the active and parasitic states **(Thiel and Smith, 2002; Jasem, 2023; Islam et al., 2012),** or the parasitic element is switched between ON and OFF states with fixed active elements using PIN diodes **(Thiel and Smith, 2002; Svantesson and Wennstrom, 2001)**. As a result, it is possible to produce a certain number of switched, steerable, and directional radiation patterns **(Thiel and Smith, 2002; Kausar et al., 2016)**.

When in receive mode, incident signals on the SPA array cause measurement voltages to be measured at the terminals of the active elements. The parasitic element produces no voltage since its terminals are shorted. However, by mutually coupling the effect of the short circuit current induced in these components to the active elements, the parasitic elements assist in directing and steering the radiation pattern generated by the array **(Thiel and Smith, 2002; Jasem, 2023)**. When evaluating the performance of these arrays, the mutual coupling is crucial. Because of this, receiving antenna arrays can perform better as direction of arrival estimators by utilizing the beam space rather than the element space. The work **(Svantesson and Wennstrom, 2001)** has shown that using a uniform circular array of monopoles acting as ON-OFF parasites and surrounding one active monopole antenna enhances the DOA estimation of the received signals by the array due to generating directive and symmetrical radiation patterns pointed in different directions. However, it has not shown the analytical expression for these patterns, which were the entries in the steering matrix of the measurements, or how the mutual coupling contributes to determining them.

In addition to the signal and noise subspaces estimated from eigen decomposing the covariance matrix of the measurements of SPA antenna arrays, a third subspace associated with very small eigenvalues will be generated due to the parasitic elements.

This work will examine the effectiveness of this third subspace, the parasitic subspace, in enhancing DOA estimation in conjunction with the MUSIC algorithm against the traditional noise subspace generated by the all-active antenna array. The evaluation considers the number of active elements and parasites within the array, the size of the array, the direction of received signals, and the number of measurement snapshots. The arrays will contain a certain number of active elements and parasitic elements. Thus, each element will be fixed in an active or parasitic state. Therefore, an array with fixed active and fixed parasite antennas (APA), examined in this work, will be a particular type of SPA array.

2. APA ARRAY IN TRANSMIT MODE

The effectiveness and benefits of employing SPA arrays in cellular communications are thoroughly discussed **(Thiel and Smith, 2002).** It is demonstrated that it is possible to

produce directed and steerable radiation patterns by utilizing these arrays as transmitting arrays. Simply switching each element in the array between the active and parasitic states will accomplish this. The radio frequency source powers the active element, while the parasitic element has short terminals. PIN diodes can be used to transition between the two states because of their extremely fast switching times (measured in nanoseconds), extremely low ON ohmic resistance, and extremely high OFF ohmic resistance. **Fig. 1** shows an equally spaced *N*-element APA array. The elements are equally spaced and distributed along the *+ve x-axis*, with the first element placed at the origin. This array is known as the APA uniform linear array (APA-ULA). In this array, there are '*r*' active elements and *N-r* parasitic elements. If $\boldsymbol{i}=\left(i_{a_1}\ i_{a_2}\ \ldots i_{a_r}\ i_{p_1}\ i_{p_2}\ \ldots i_{p_{N-r}}\right)^T$, is the column vector of the coupled currents in the array's elements, with i_a and i_p being the active and parasitic currents, respectively, the expression for the total radiated *H*-plane electric field of the array in terms of the element currents is **(Thiel and Smith, 2002):**

$$E_t(\mathrm{r},\theta,\phi)=\gamma(\theta)\boldsymbol{i}^T\boldsymbol{a}(\phi) \quad (1)$$

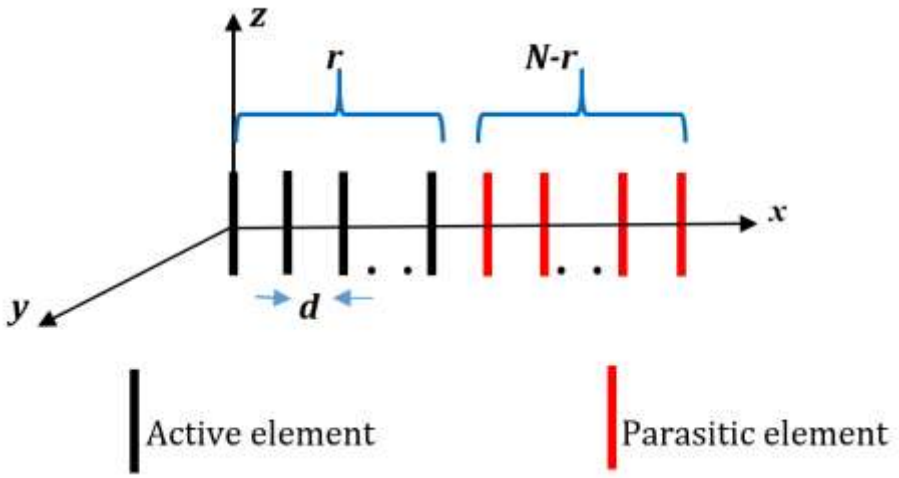

Figure 1. An APA-ULA consisting of *N* half-wave dipole antennas. The number of active elements is *r*, and the number of parasites is *N-r*.

where

$$\gamma(\theta)=\frac{j\omega\mu}{2\pi kR}\frac{cos\left(\frac{\pi}{2}cos\theta\right)}{sin\theta}$$

with ω being the radian frequency of the power supply, μ being the permittivity, k being the wave number, and R is the distance to the observation point. $\boldsymbol{a}(\phi)=\left(1\ e^{jkdcos(\phi)}\ e^{j2kdcos(\phi)}\ldots e^{j(N-1)kdcos(\phi)}\right)^T$ is the steering column vector, and $(.)^T$ is the transpose operation. **Fig. 2** illustrates the azimuthal radiation patterns for different sets of active and parasitic elements of an APA-ULA consisting of five half-wave dipoles with interelement spacing $d=0.125\ \lambda$. It can be seen from **Fig. 2** that increasing the number of active elements contributes to improving the gain of the array and reducing the front-to-back ratio.

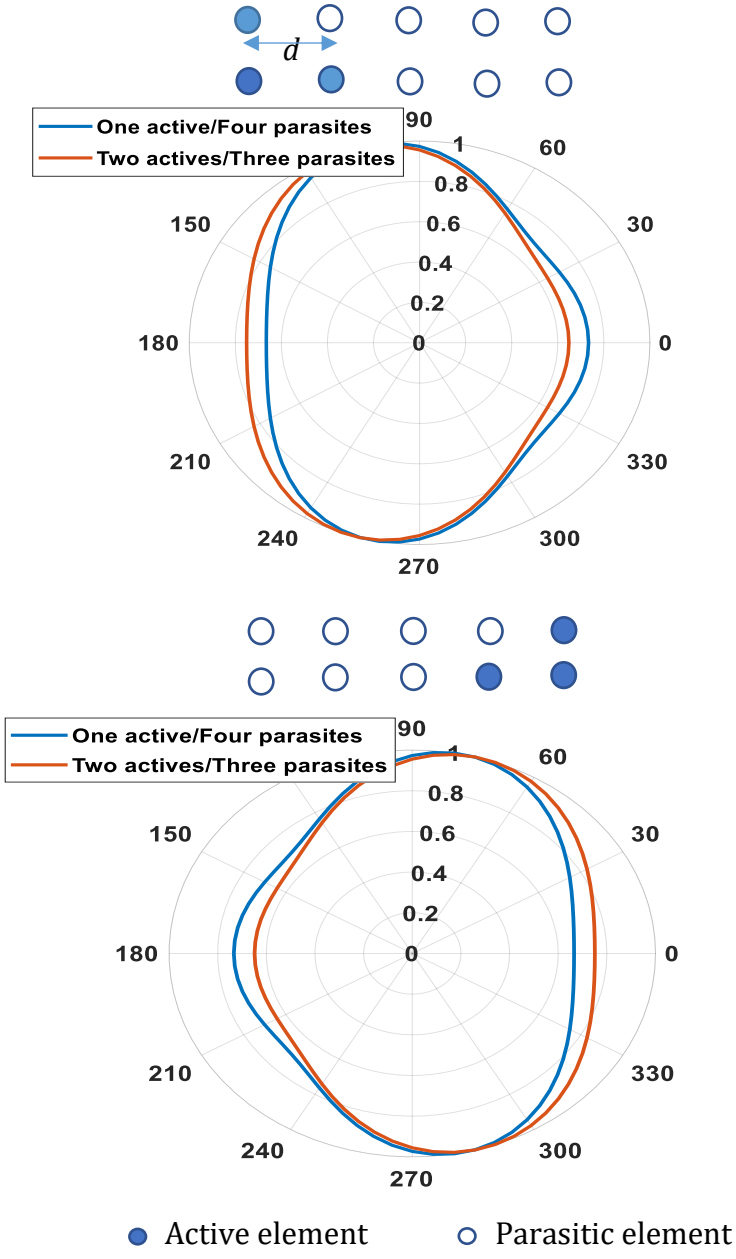

Figure 2. Azimuthal radiation patterns for different sets of active and parasitic elements of an APA-ULA consisting of five half-wave dipoles with inter-element spacing $d = 0.125\ \lambda$

3. DATA MODEL OF A RECEIVING APA-ULA ARRAY

This section studies the data model of an N-element APA-ULA acting as a receiving antenna array. The array structure is the same as the one shown in **Fig. 1**. The antenna elements are half-wave dipole antennas with a diameter of $a << \lambda$, where λ is the wavelength of the received signal. This condition ensures that the assumption of sinusoidal current distribution in the dipole is valid, with the maximum value at the center of the dipole **(Balanis, 2016)**. First, suppose that the array consists of N all-active elements receiving M narrowband signals. The

data model for the measurements that are developed at the terminals of the array elements will be **(Schmidt, 1986; Roy and Kailath, 1989; Svantesson and Wennstrom, 2001):**

$$\mathbf{x}(t) = \boldsymbol{CA}(\phi)\boldsymbol{s}(t) + \boldsymbol{n}(t) \quad (2)$$

where, $\mathbf{x}(t) \in \mathbb{C}^{N\times 1}$ is the vector of the array's measurement. $\boldsymbol{C} \in \mathbb{C}^{N\times N}$ is the mutual coupling matrix. $\boldsymbol{A}(\phi) = [a(\phi_1)\ a(\phi_2). \ . \ . a(\phi_M)] \in \mathbb{C}^{N\times M}$ is the steering matrix with

$\boldsymbol{a}(\phi_m) = \left(1 \quad e^{jkdcos\phi_m} \quad e^{j2kdcos\phi_m} \ . \ . \ . \quad e^{j(N-1)kdcos\phi_m}\right)^T \quad m = 1,2,..,M$ being the response vector of the array to the received signal m. $\boldsymbol{s}(t) \in \mathbb{C}^{M\times 1}$

is the vector of the strength of the received signals. $\boldsymbol{n}(t) \in \mathbb{C}^{\boldsymbol{N\times 1}}$ is the noise vector**.** Assuming that there is no coherency between the received signals and the noise and between the signals themselves, the covariance matrix $\boldsymbol{R} \in \mathbb{C}^{N\times N}$ of the measurement is calculated from:

$$\boldsymbol{R} = E(\mathbf{x}(t)\mathbf{x}(t)^H) = \boldsymbol{CA}(\phi)E(\boldsymbol{ss^H})\boldsymbol{A}(\phi)^{\boldsymbol{H}}\boldsymbol{C^H} + E(\boldsymbol{n(t)n(t)^H}) \quad (3)$$

where $E(.)$ is the expectation operator and $(.)^H$ is the Hermitian operation. Due to the presumption that received signals and noise are uncorrelated, it should be noted that the cross-product terms have disappeared. In addition, if the received signals are not correlated with each other, then the expectation of the covariance matrix of the strength of the received signals yields a diagonal matrix $\boldsymbol{S} \in \mathbb{C}^{M\times M}$ with the power of the signals on the diagonal **(Svantesson and Wennstrom, 2001)**. Also, it is assumed that the noise is AWGN with normal distribution, i.e., $E(\boldsymbol{nn^H}) = \sigma^2\boldsymbol{I}$**,** where σ^2 is the noise power and $\boldsymbol{I} \in \mathbb{C}^{\boldsymbol{N\times N}}$ is the identity matrix **(Chandran, 2005; Chen et al., 2010)**. Taking the eigen decomposition of $\boldsymbol{R}$ in Eq. (3) yields:

$$\boldsymbol{R} = \boldsymbol{CA}(\phi)\boldsymbol{SA}(\phi)^{\boldsymbol{H}}\boldsymbol{C^H} + \sigma^2\boldsymbol{I} = \boldsymbol{E_s\Lambda_sE_s^H} + \boldsymbol{E_n\Lambda_nE_n^H} \quad (4)$$

In Eq. (4), $\boldsymbol{E_s} = \left[\boldsymbol{e}_{s,1}\ \boldsymbol{e}_{s,2}\ .\ .\boldsymbol{e}_{s,M}\right] \in \mathbb{C}^{N\times M}$, $\boldsymbol{E_n} = \left[\boldsymbol{e}_{n,M+1}\ \boldsymbol{e}_{n,M+2}\ .\ .\boldsymbol{e}_{n,N}\right] \in \mathbb{C}^{N\times(\boldsymbol{N-M})}$ are signal and noise subspaces, respectively, with $\boldsymbol{e}_s$ and $\boldsymbol{e}_n$ being the signal and noise vectors, respectively. $\boldsymbol{E_s}$ and $\boldsymbol{E_n}$ are orthonormal matrices **(Foutz et al., 2008)**. These two subspaces are orthogonal to each other. $\boldsymbol{\Lambda_s} \in \mathbb{R}^{M\times M}$, $\boldsymbol{\Lambda_n} \in \mathbb{R}^{(N-M)\times(N-M)}$ are diagonal matrices containing the eigenvalues of the signal subspace and the noise subspace, respectively. Note that the eigenvalues of the two subspaces are real and non-negative since the covariance matrix $\boldsymbol{R}$ is positive-definite **(Horn and Johnson, 2013; Golub and Van Loan, 2013)**. Also, the eigenvalues of the noise subspace are equal to σ^2. Thus, the eigenvalues of $\boldsymbol{R}$ will be ordered as $\Lambda_1 \geq \Lambda_2 \cdots \Lambda_M \geq \Lambda_{M+1} = \Lambda_{M+2} = \cdots = \Lambda_N$. When the measurements are noiseless, the eigenvalues, $\Lambda_{M+1} = \Lambda_{M+2} = \cdots = \Lambda_N$, will have zero values. When the measurements are noisy, the noise subspace resides in the null space of the matrix $\boldsymbol{CA}(\phi)\boldsymbol{SA}(\phi)^{\boldsymbol{H}}\boldsymbol{C^H}$**.** However**,** the rank of $\boldsymbol{R}$ in Eq. (4) is one, i.e., rank ($\boldsymbol{R}$)=1. Therefore, the full rank sample of $\boldsymbol{R}$ is practically obtained by averaging a very large number of measurement snapshots Q to have an unbiased DOA estimation, i.e.,

$$\boldsymbol{R} = \frac{\boldsymbol{1}}{\boldsymbol{Q}}\ \sum_{\boldsymbol{i=1}}^{\boldsymbol{Q}} \mathbf{x}\,(t_i)\ \mathbf{x}(t_i)^{\boldsymbol{H}} = \boldsymbol{\hat{E}_s\hat{\Lambda}_s\hat{E}_s^H} + \boldsymbol{\hat{E}_n\hat{\Lambda}_n\hat{E}_n^H} \quad (5)$$

where $(\hat{.})$ means the estimated value. Note that the eigenvalues, $\hat{\Lambda}_{M+1}, \hat{\Lambda}_{M+2}, \cdots \hat{\Lambda}_N$, are not necessarily equal due to perturbations in noise. As a result, the signal subspace may merge into the noise subspace, especially when the sample size is small or when the signals are received with a low signal-to-noise ratio **(Shaghaghi and Vorobyov, 2015)**.
In the case of an *N*-element APA-ULA array, suppose that the first *r* elements are active, and the other *N-r* elements are parasites. The active element is the element loaded by an impedance Z_L at its center, while the terminals of the parasitic element are short-circuited. Suppose the array receives *M* narrowband signals. The eigen decomposition of the covariance matrix of the measurements $\boldsymbol{R}_{APA}$ will also consist of signal and noise subspaces, the same subspaces as in Eq. (4). However, $\boldsymbol{R}_{APA}$ involves several rows and columns with zero values. These entries are due to the zero entries in the measurement vector $\mathbf{x}(t)$ corresponding to the parasites**.** Therefore, in addition to the signal and noise subspaces, the covariance matrix's spectral decomposition also contains an additional subspace, $\boldsymbol{E}_{\boldsymbol{PAR}}$, with very small eigenvalues (almost zero) corresponding to the parasitic elements. The number of these eigenvalues and associated vectors equals the number of parasites, i.e.,

$$\boldsymbol{R}_{APA} = \boldsymbol{E}_{\boldsymbol{s}}\boldsymbol{\Lambda}_{\boldsymbol{s}}\boldsymbol{E}_{\boldsymbol{s}}^{\boldsymbol{H}} + \boldsymbol{E}_{\boldsymbol{n}}\boldsymbol{\Lambda}_{\boldsymbol{n}}\boldsymbol{E}_{\boldsymbol{n}}^{\boldsymbol{H}} + \boldsymbol{E}_{\boldsymbol{PAR}}\boldsymbol{\Lambda}_{\boldsymbol{PAR}}\boldsymbol{E}_{\boldsymbol{PAR}}^{\boldsymbol{H}} \tag{6}$$

where, $\boldsymbol{E}_{\boldsymbol{s}} = \left[\boldsymbol{e}_{s,1}\ \boldsymbol{e}_{s,2}\ \ldots \boldsymbol{e}_{s,M}\ \right] \in \mathbb{C}^{\boldsymbol{N}\times\boldsymbol{M}}$, $\boldsymbol{E}_{\boldsymbol{n}} = \left[\boldsymbol{e}_{n,M+1}\ \boldsymbol{e}_{n,M+2}\ldots \boldsymbol{e}_{n,r}\right] \in \mathbb{C}^{\boldsymbol{N}\times(\boldsymbol{r}-\boldsymbol{M})}$, and $\boldsymbol{E}_{\boldsymbol{PAR}} = \left[\boldsymbol{e}_{PAR,r+1}\ \boldsymbol{e}_{PAR,r+2}\ldots \boldsymbol{e}_{PAR,N}\right] \in \mathbb{C}^{\boldsymbol{N}\times(\boldsymbol{N}-\boldsymbol{r})}$ are the signal, the noise, and the parasitic subspaces, respectively. Therefore, the eigenvalues: $\hat{\Lambda}_{r+1}, \hat{\Lambda}_{r+2}, \cdots \hat{\Lambda}_N$ corresponding to the subspace $\widehat{\boldsymbol{E}}_{\boldsymbol{PAR}}$, which can be estimated practically from eigen decomposing $\boldsymbol{R}_{APA}$, are almost equal to zero, i.e., $\hat{\Lambda}_{r+1} \approx \hat{\Lambda}_{r+2} \approx \cdots \cong \hat{\Lambda}_N \cong 0$, and complete orthogonality between $\widehat{\boldsymbol{E}}_{\boldsymbol{PAR}}$ and the column space of the matrix $\boldsymbol{A}(\phi)$, i.e., $col(\boldsymbol{A}(\phi))$, will be ensured**.** Note that a subset of this subspace could be used rather than the subspace itself to have better results since a subset of a subspace is the subspace itself **(Hefferon, 2017)**. Thus, using the subset of the subspace $\widehat{\boldsymbol{E}}_{\boldsymbol{PAR}}$ associated with the lowest eigenvalues contributes to the possibility of having DOA estimation with super-resolution despite the very small number of measurement snapshots or the size of the array aperture being small. These advantages contribute to APA arrays outweighing all-active (traditional) arrays since the spectrum of the MUSIC algorithm is significantly improved, as will be seen by different simulations in the section on the results.

4. MUTUAL COUPLING IN APA ARRAYS

The essential characteristic of SPA or APA arrays is mutual coupling. The form and directivity of the radiation pattern generated from these arrays operating in transmitting mode are determined mainly by the coupled energy from the active element to the parasitic element and back to the active element. In the receiving mode, the mutual coupling links the energy that the received signal induces in the parasitic element into the active element, adding (constructively or destructively) this energy to the energy that the received signal alone induced in the receiving active element. For the case of all-active antenna arrays, many mutual coupling models, such as those in **(Gupta and Ksienski, 1983; Hui, 2004; Lui et al., 2009.; Hui and Lu, 2006; Yu and Hui, 2011)** have been developed**.** However, these models

do not suit SPA or APA arrays due to singularities that occur when using the $Z_L = 0$ condition for the parasites. The mutual coupling model in **(Yamada et al., 2005)** considers the effect of the scattered or retransmitted fields emanating from the array's elements when receiving the electromagnetic fields. However, the method for calculating the corresponding mutual impedance due to this effect has not been shown**.** The CVUC model has been put forth by **(Jasem, 2020)** to represent the mutual coupling phenomena between antenna array elements. This model relates the antenna-coupled load voltages developed at the antenna terminals to the free-coupling currents produced in the antennas only by the received signals. The expression for this model is:

$$\mathbf{v_L} = (\boldsymbol{K} + \boldsymbol{F}\boldsymbol{Y}^{-1})\mathbf{u} = \boldsymbol{C}\mathbf{u} \tag{7}$$

The column vectors $\mathbf{v_L} = \left(v_{L,1}\ v_{L,2}\ .\ .\ v_{L,N}\right)^{\boldsymbol{T}}$ and $\mathbf{u} = (I_1\ I_2\ .\ .\ I_N)^{\boldsymbol{T}}$ represent, respectively, the coupled load voltages and the free-coupling currents of the antenna elements in an array operating in receiving mode. The matrices $\boldsymbol{K}$, $\boldsymbol{F}$, and $\boldsymbol{Y}$ are as follows **(Jasem, 2020):**

$$\boldsymbol{K} = \begin{bmatrix} Z_{11}+Z_{L,1} & 0 & 0 & \dots & 0 \\ 0 & Z_{22}+Z_{L,2} & 0 & \dots & 0 \\ \vdots & \vdots & \vdots & \dots & \vdots \\ 0 & 0 & 0 & \dots & Z_{NN}+Z_{L,N} \end{bmatrix} \tag{8}$$

$$\boldsymbol{F} = \begin{bmatrix} -Z_{11} & Z_{12} & . & . & Z_{1N} \\ Z_{21} & -Z_{22} & . & . & Z_{2N} \\ . & . & . & . & . \\ . & . & . & . & . \\ Z_{N1} & Z_{N2} & . & & -Z_{NN} \end{bmatrix} \tag{9}$$

$$\boldsymbol{Y} = \begin{bmatrix} 1 & \frac{-Z_{12}}{Z_{11}+Z_{L,1}} & . & . & \frac{-Z_{1N}}{Z_{11}+Z_{L,1}} \\ \frac{-Z_{21}}{Z_{22}+Z_{L,2}} & 1 & . & . & \frac{-Z_{2N}}{Z_{22}+Z_{L,2}} \\ . & . & . & . & . \\ . & . & . & . & . \\ \frac{-Z_{N1}}{Z_{NN}+Z_{L,N}} & \frac{-Z_{N2}}{Z_{NN}+Z_{L,N}} & . & . & 1 \end{bmatrix} \tag{10}$$

where Z_{pp} is the self-impedance of element p, and Z_{pq} is the mutual impedance between elements p and q. The CVUC model suits APA arrays since the column vector $\mathbf{v_L}$ will contain zero entries corresponding to the parasites as a result of applying the parasitic condition (by substituting $Z_L = 0$ as the load of parasites) into the RHS of Eq. (7). Thus, the vector $\mathbf{v_L}$ contains r-measured values of load voltages and N-r zeros.

5. DOA ESTIMATION USING APA ARRAYS.

To estimate the one-dimensional DOA of the signals received by all-active antenna arrays, the estimated noise subspace $\widehat{\boldsymbol{E}}_{\boldsymbol{n}}$ calculated from Eq. (5) can be used in the MUSIC cost function, which is **(Schmidt, 1986; Svantesson and Wennstrom, 2001):**

$$P_{MUSIC}(\phi) = \frac{1}{a^H(\phi)C^H\widehat{E}_n\widehat{E}_n^H Ca(\phi)} \tag{11}$$

The structure of the search vector $a(\phi)$ is similar to each column of the steering matrix $\boldsymbol{A}(\boldsymbol{\phi})$ in Eq. (2) but calculated for the set of angles $\{-\pi, \pi\}$. The mutual coupling matrix $\boldsymbol{C}$ might be the CVUC model defined in Eq. (7), which is assumed to be known. The cost function in Eq. (11) searches for the peaks that occur when the set M of the search vectors $\boldsymbol{Ca}(\phi_{\boldsymbol{m}})$ is orthogonal to the estimated noise subspace $\widehat{\boldsymbol{E}}_{\boldsymbol{n}}$. The cost function in Eq. (11) is based on the fact that the column space of the coupled steering matrix $\boldsymbol{CA}(\phi)$ of Eq. (2) is orthogonal to the noise space, i.e., $\mathcal{R}\big(\boldsymbol{CA}(\phi)\big) \perp \boldsymbol{E_n}$ or $\boldsymbol{A}(\phi)^{\boldsymbol{H}}\boldsymbol{C}^{\boldsymbol{H}}\boldsymbol{E_n} = \boldsymbol{0}$, where the size of the zero matrix $\boldsymbol{0}$ is $M \times (N - M)$.

Estimating the DOA using Eq. (11) may result in poor resolution under some conditions. The small size of the array's aperture and the spatially closed received signals deteriorate the resolution of the DOA estimation. Additionally, when the received signals have a low S/N ratio, the resolution of the DOA estimation may be affected by the influence of a significant perturbation of the noise eigenvalues. In the last case, part of the signal subspace merges into the noise subspace, which may lead to failure in the precise detection of the DOAs **(Shaghaghi and Vorobyov, 2015; Zhang et al., 2021)**. As a result of the above cases, some of the eigenvectors of the estimated noise subspace will not be completely orthogonal to the corresponding DOA search vector $\boldsymbol{Ca}(\phi)$. However, estimating the DOAs using $\widehat{\boldsymbol{E}}_{\boldsymbol{PAR}}$, the parasitic subspace, in Eq. (11) instead of $\widehat{\boldsymbol{E}}_{\boldsymbol{n}}$ overcomes these adverse effects. All eigenvectors of $\widehat{\boldsymbol{E}}_{\boldsymbol{PAR}}$ are completely orthogonal to the column space of $\boldsymbol{CA}(\phi)$ of Eq. (2). As a result, superiority over using $\widehat{\boldsymbol{E}}_{\boldsymbol{n}}$ in DOA estimation will be obtained when using $\boldsymbol{E}_{\boldsymbol{PAR}}$. As a result, Eq. (11) can be modified as follows by taking advantage of the subspace $\boldsymbol{E}_{\boldsymbol{PAR}}$ produced by APA arrays:

$$P_{MUSIC}(\phi) = \frac{1}{\boldsymbol{a}^H(\phi)\boldsymbol{C}^{\boldsymbol{H}}\widehat{\boldsymbol{E}}_{\boldsymbol{PAR}}\widehat{\boldsymbol{E}}_{\boldsymbol{PAR}}^{\boldsymbol{H}}\boldsymbol{Ca}(\boldsymbol{\phi})} \tag{12}$$

Thus, the MUSIC spectrum will show peaks at any ϕ_m when $\boldsymbol{Ca}(\phi_m)$ is orthogonal to $\boldsymbol{E}_{\boldsymbol{PAR}}$.

6. SIMULATION RESULTS

In the following simulations, the capability of the APA array as a high-resolution direction-finding array will be examined. Also, the superiority and advantages of using $\widehat{\boldsymbol{E}}_{\boldsymbol{PAR}}$ over $\widehat{\boldsymbol{E}}_{\boldsymbol{n}}$ will be depicted. The array is APA-ULA with eight half-wave dipoles, as shown in **Fig. 1**. The element spacing is $d = 0.2\ \lambda$. The array receives two signals coming from the directions $\phi_1 = 70°, \phi_2 = 72°$. The signals are assumed to be incident in the *x-y* plane, and the signal-to-noise ratio of each signal is S/N= 10 dB. The mutual coupling, the CVUC model, is assumed to be known. **Fig. 3** shows the MUSIC spectrums for this scenario, with the array having four active elements, i.e., $r = 4$, and four parasites. The plots in this figure illustrate a comparison

between the resolution of DOA estimations obtained from Eq. (11) and Eq. (12). Five runs, $L = 5$, are executed for the measurements, with each run involving Q=500 snapshots. **Fig. 3** illustrates that using the subspace $\widehat{\boldsymbol{E}}_{\boldsymbol{PAR}}$ generated by the parasites in an APA-ULA array is capable of estimating the DOAs of the received signals with a resolution much higher than using the noise subspace $\widehat{\boldsymbol{E}}_{\boldsymbol{n}}$. The plots in this figure show that different runs result in MUSIC spectrums that coincide in the case of using $\widehat{\boldsymbol{E}}_{\boldsymbol{PAR}}$. In contrast, a poor coincidence occurs when Eq. (11) is used. **Fig. 3C** depicts that using a subset of the subspace $\widehat{\boldsymbol{E}}_{\boldsymbol{PAR}}$ **,** specifically the last two vectors of $\widehat{\boldsymbol{E}}_{\boldsymbol{PAR}}$, i.e., $\left[\hat{\boldsymbol{e}}_{PAR,N-1}\ \hat{\boldsymbol{e}}_{PAR,N}\right]$ the active elements, being the first r elements, result in a MUSIC spectrum with a super-resolution to the received signals. This plot illustrates that the subset of $\widehat{\boldsymbol{E}}_{\boldsymbol{PAR}}$ associated with the lowest eigenvalues can be used to estimate the DOAs as if the measurements were noiseless. The plots in **Fig. 4** show the DOA estimations for two signals coming from the directions $\phi_1 = 20°, \phi_2 = 22°$ and received by the same array used to produce **Fig. 3**. This figure illustrates that the APA-ULA array performs well in estimating the DOA for signals coming from the end-fire direction and can also be achieved with very high resolution**.** The coincidence in plots for different runs of MUSIC spectrums when using $\widehat{E}_{PAR}$. This figure confirms the effectiveness of the parasitic subspace, although the signals were received from critical directions. Also, it is shown in part (c) of this figure that using the last two vectors of $\widehat{\boldsymbol{E}}_{\boldsymbol{PAR}}$ results in a DOA estimation with a super-resolution. In contrast, using Eq. (11) results in poor resolution. However, it was required that the signal-to-noise ratio of the received signal for this scenario be S/N= 35 dB because the signals are received by the array from its end-fire direction. Also, the power of the radiation pattern of the array on its right side is low due to the effect of parasites.

The MUSIC spectrums in **Fig. 5** illustrate the ability of using the APA array to detect the DOA of received signals when their number is equal to the number of active elements. The array is the same array used to obtain the MUSIC spectrums shown in **Fig. 3**, but the number of active elements is now only two. **Fig. 5a** shows DOA estimation when the whole subspace $\widehat{\boldsymbol{E}}_{\boldsymbol{PAR}}$ is used in Eq. (12). Also, **Fig. 5b** shows the MUSIC spectrum for the same array and the same received signals, but the last two vectors of $\widehat{\boldsymbol{E}}_{\boldsymbol{PAR}}$ is now used. Note that the noise subspace does not exist in this scenario due to the number of received signals and the number of active elements being equal. Thus, APA arrays outperform all-active antenna arrays in avoiding the compulsory condition that the number of measured responses should be greater than the number of received signals **(Chandran, 2005; Chen et al., 2010; Schmidt, 1986).**

As previously mentioned in **Section 3**, the number of snapshots, Q, must be large enough for an unbiased DOA estimation. However, when using a subset of the subspace $\widehat{\boldsymbol{E}}_{\boldsymbol{PAR}}$ that is associated with the smallest eigenvalues in Eq. (12), this condition will be unnecessary. **Fig. 6** demonstrates this fact. It is shown in this figure that using the subset of $\widehat{\boldsymbol{E}}_{\boldsymbol{PAR}}$ has succeeded in obtaining super-resolution DOA estimation with the number of snapshots equal only to Q=10, while the noise subspace, $\widehat{\boldsymbol{E}}_{\boldsymbol{n}}$, fails to do so.

Thus, if the mutual coupling is known, the APA-ULA can be used as a direction-finding array to estimate the DOA of received signals with very high or super-resolution, regardless of the directions of the signals, the array's aperture size, the number of active measurements, or the number of measurement snapshots. This is demonstrated clearly in **Fig. 3** to **Fig. 6**.

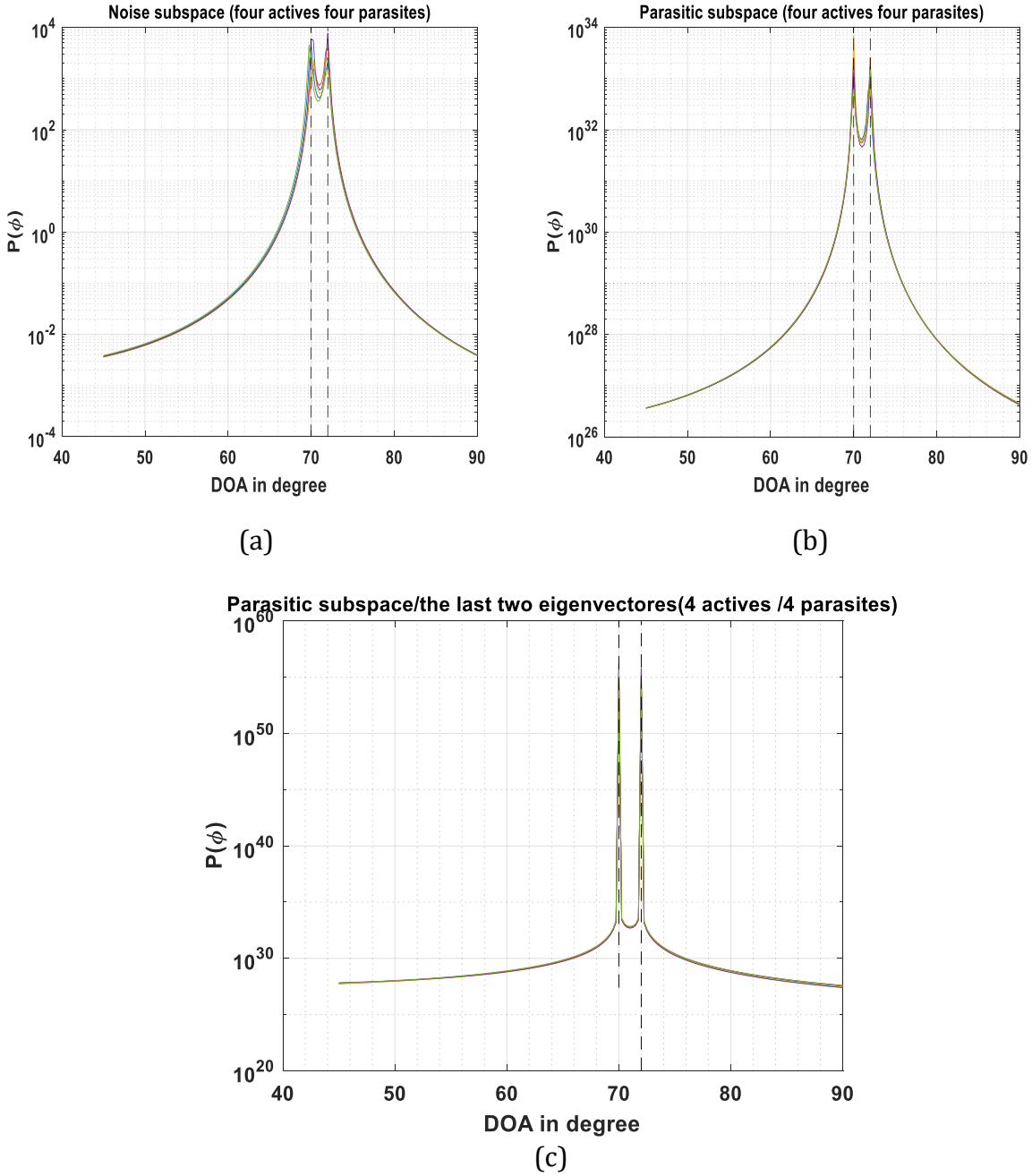

Figure 3. MUSIC spectrums, $P(\phi)$, for two signals coming from the directions $\phi_1 = 70°, \phi_2 = 72°$ with S/N= $10dB$, and received by an eight-elements half-wave dipole APA-ULA. $d = 0.2\ \lambda$, $L = 5$, and $Q = 500$. (a) Using the subspace $\widehat{\boldsymbol{E}}_{\boldsymbol{n}}$. (b) Using the subspace $\widehat{\boldsymbol{E}}_{\boldsymbol{PAR}}$. (c) Using the last two vectors of the subspace $\widehat{\boldsymbol{E}}_{\boldsymbol{PAR}}$.

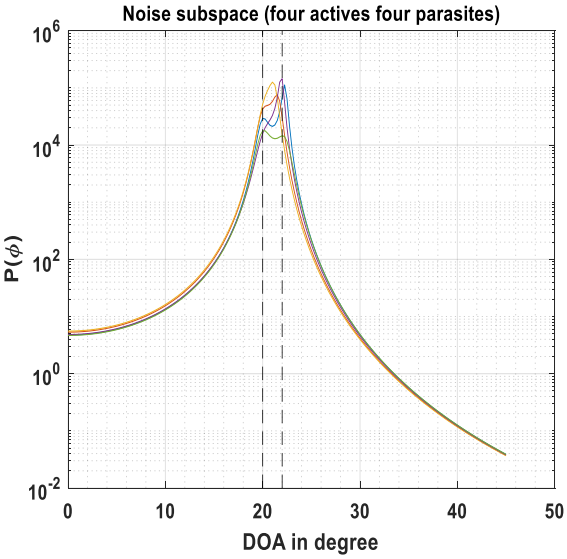

(a)

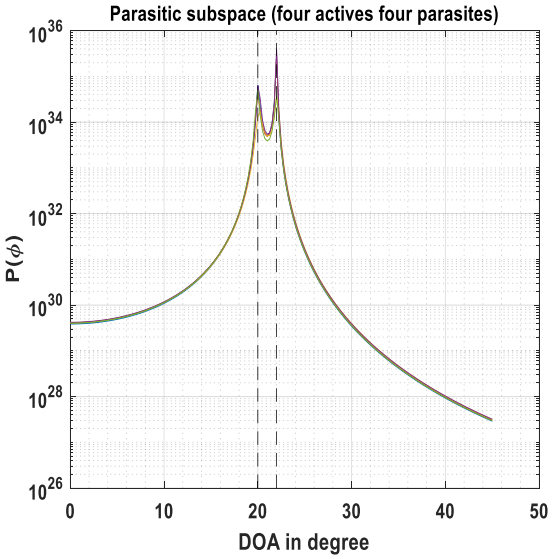

(b)

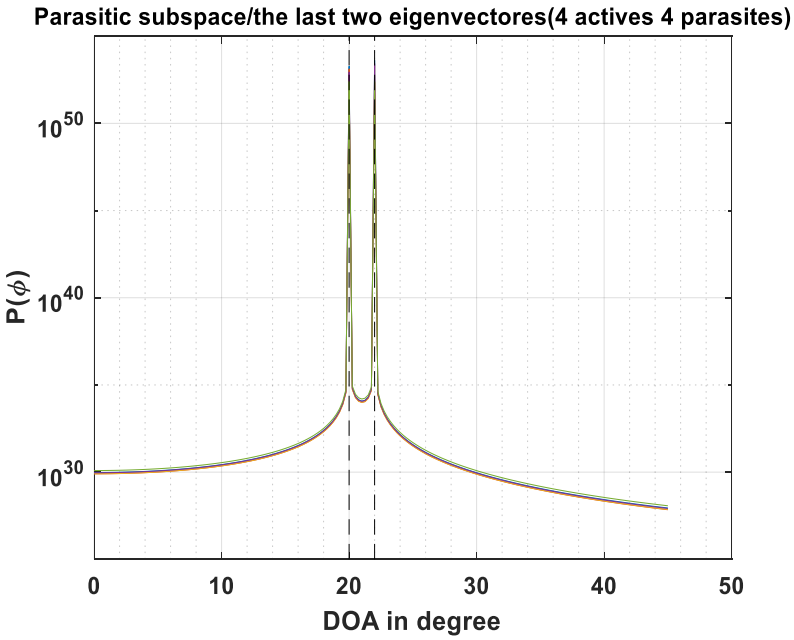

(c)

Figure 4. MUSIC spectrums, $P(\phi)$, for two signals coming from the directions $\phi_1 = 20°, \phi_2 = 22°$ and received by the same array used for the plots of **Fig. 3**. S/N= $35dB$. (a) Using the subspace $\widehat{\boldsymbol{E}}_{\boldsymbol{n}}$. (b)Using the subspace $\widehat{\boldsymbol{E}}_{\boldsymbol{PAR}}$. (c)Using the last two vectors of the subspace $\widehat{\boldsymbol{E}}_{\boldsymbol{PAR}}$.

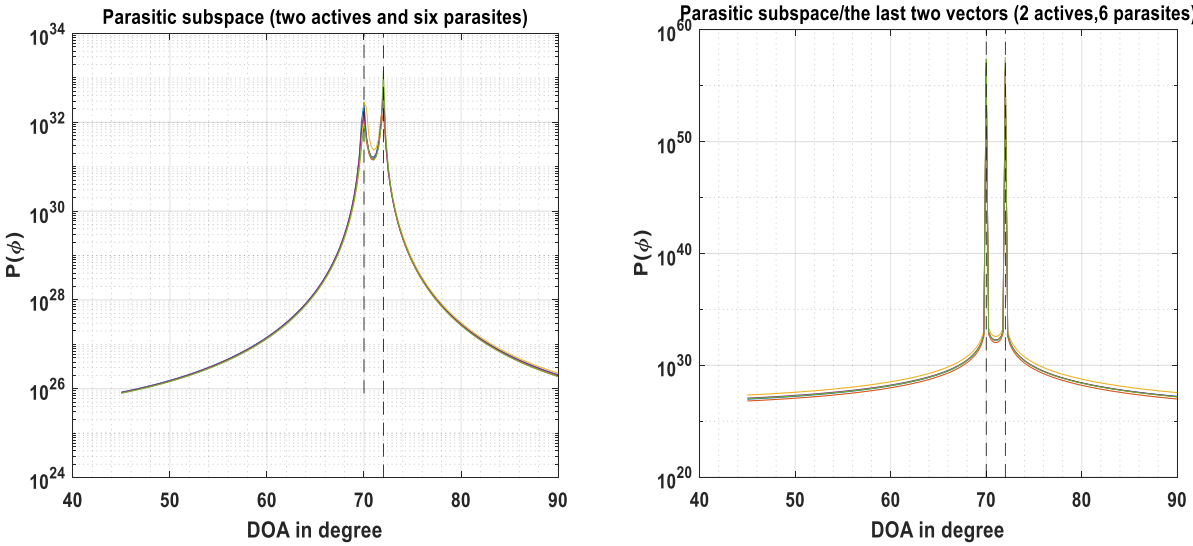

(a) (b)

Figure 5. MUSIC spectrums, $P(\phi)$, for the same scenario as in **Fig. 3**, but the number of active elements is only two. (a) Using the subspace $\widehat{\boldsymbol{E}}_{\boldsymbol{PAR}}$. (b) Using the last two vectors of the subspace $\widehat{\boldsymbol{E}}_{\boldsymbol{PAR}}$

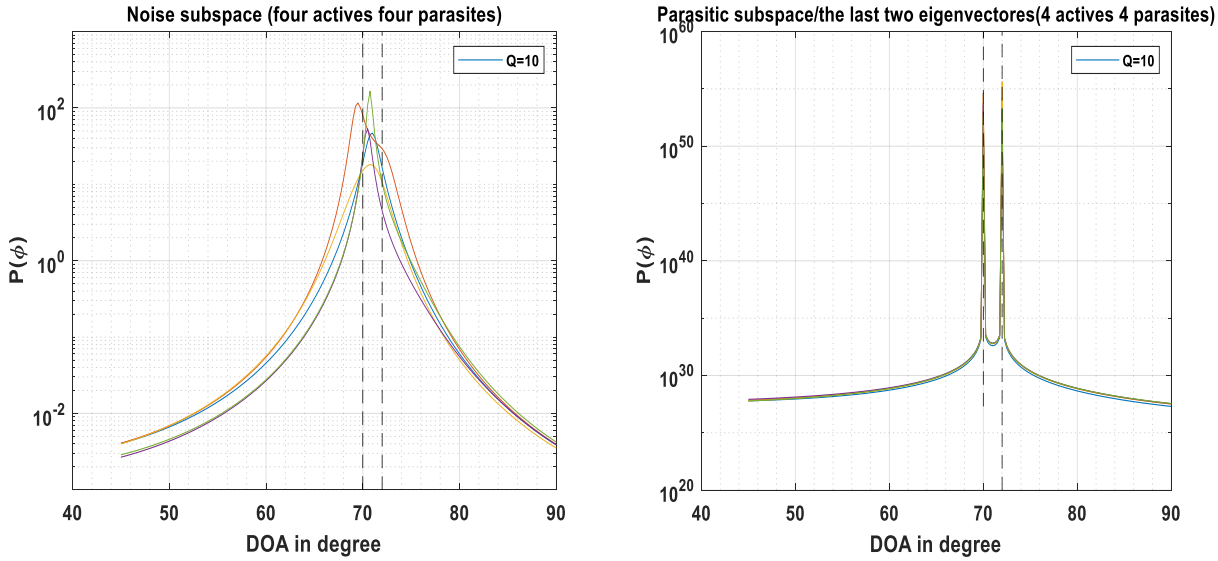

(a) (b)

Figure 6. MUSIC spectrums, $P(\phi)$, for the same scenario used to obtain the plots in **Fig. 3**, but the number of measurement snapshots is Q=10. (a) Using the subspace $\widehat{\boldsymbol{E}}_{\boldsymbol{n}}$. (b) using the last two vectors of the subspace $\widehat{\boldsymbol{E}}_{\boldsymbol{PAR}}$.

Fig. 7a shows the root mean square error (RMSE) criterion when using parasitic and noise subspaces. The *RMSE* is defined as:

$$RMSE = \sqrt{\frac{\sum_{i=1}^{L}(\hat{\phi}-\phi)^2}{L}} \tag{13}$$

where, $\hat{\phi}$, ϕ, are, respectively, the estimated and the actual values of the DOA, and L is the number of runs. The *RMSE* is plotted against different values of SNR. The array consists of six elements with three active elements. The signal is incident on the array from the direction $\phi = 5^o$, i.e., from the end-fire direction. The number of runs was $L = 100$, and with snapshots, $Q = 50$ for each run has been used to plot this figure. **Fig. 7b** compares between $\widehat{\boldsymbol{E}}_{\boldsymbol{PAR}}$ and $\widehat{\boldsymbol{E}}_{\boldsymbol{n}}$ regarding the RMSE criterion for the same received signal but when the array consists of two actives and three parasites. The plots in **Fig. 7** demonstrate that the RMSE curve, when using the subspace, $\widehat{\boldsymbol{E}}_{\boldsymbol{PAR}}$ is much lower than the RMSE curve when using the subspace, $\widehat{\boldsymbol{E}}_{\boldsymbol{n}}$ regardless of the number of active or parasitic elements. Hence, a very small difference between the estimated and the actual DOA can be obtained over a wide range of S/N ratios when using the parasitic subspace.

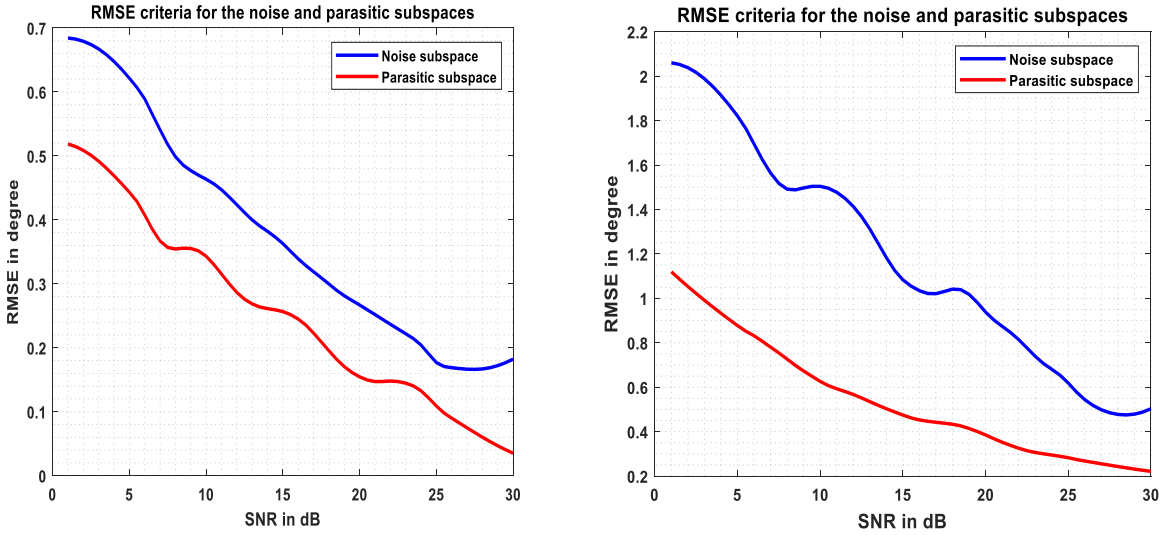

(a) (b)

Figure 7. RMSE plots versus SNR for a signal coming from the direction $\phi = 5^o$ and incident on an APA-ULA antenna array. $d = 0.2\ \lambda$, L=100, and $Q = 50$. The array consists of (a) three active elements and three parasites. (b) two active elements and three parasites.

7. CONCLUSIONS

The enhancement in DOA estimation by using APA-ULA arrays in conjunction with the MUSIC algorithm is studied in this work. An APA array consists of a certain number of active elements, and the rest of the elements are parasites. The terminal of the parasitic element is short-circuited, while a load loads the terminal of the active element. The measurements that represent the response to the received signals by the APA arrays are developed at the loaded terminals of the actives. The outcomes of this work can be concluded as follows:

- The main advantage of APA arrays, when used as direction finders, is that they generate a parasitic subspace associated with very small eigenvalues (almost zero values). This subspace is obtained by eigen decomposing the covariance matrix of the array's measurement. Using this subspace results in a MUSIC spectrum with very high resolution compared to the MUSIC spectrum obtained when using the noise subspace.

Also, using a subset of the parasitic subspace results in super-resolution MUSIC spectrums. It is shown that this outcome has been achieved for arrays with small apertures. Also, it is found that the direction of the received signals does not affect the performance of the parasitic subspace.

- The condition of the number of received signals, which should be less than the number of the array's elements when using all-active antenna arrays as direction finders, has been avoided when the parasitic subspace is considered in the case of APA arrays.
- It can be possible to achieve unbiased DOA estimation with a very small number of measurement snapshots when using $\widehat{\boldsymbol{E}}_{\boldsymbol{PAR}}$.
- Using the parasitic subspace significantly reduces the difference between the estimated and true DOA when using the RMSE criterion.

In conclusion, the APA-ULA array has enhanced the estimation of DOA of received signals under different conditions and overcomes some constraints. Thus, the advantages of these arrays can be effectively exploited when it is required to have precise knowledge about the direction of the users in a dense and noisy environment. These benefits are greatly useful in mobile communication. Also, APA arrays can be fabricated with less hardware when compared with traditional all-active antenna arrays.

REFERENCES

Balanis, C.A., 2016. *Antenna theory: analysis and design.* 4th ed. John Wiley and Sons.

Chandran, S., 2005. *Advances in direction-of-arrival estimation.* Artech House, INC.

Chen, Z., 2019. Review of direction of arrival estimation algorithms for partial discharge localisation in transformers. *IET Science, Measurement and Technology,* 13(4), pp. 529-535. Doi:10.1049/iet-smt.2018.5297.

Chen, Z., Gokeda, G., and Yu, Y., 2010. *Introduction to direction-of-arrival estimation.* Boston: Artech House.

El Zooghby, A., 2005. *Smart Antenna Engineering.* London: Artech house.

Eranti, P.K., and Barkana, B.D., 2022. An overview of direction-of-arrival estimation methods using adaptive directional time-frequency distributions. *Electronics,* 11(9), P. 1321. Doi:10.3390/electronics11091321.

Ferreira, T.N., Netto, S.L., and Diniz, P.S.R., 2008. Beamspace covariance-based DoA estimation. *IEEE 9th Workshop on Signal Processing Advances in Wireless Communications,* Recife, Brazil, pp. 136-140. Doi:10.1109/SPAWC.2008.4641585.

Foutz, J., Spanias, A., and Banavar, M.K., 2008. *Narrowband direction of arrival estimation for antenna arrays.* Morgan and Claypool Publishers.

Golub, G.H., and Van Loan, C.F., 2013. *Matrix Computations.* 4th ed. Baltimore: The Johns Hopkins University Press.

Gupta, I.J., and Ksienski, A.A., 1983. Effect of mutual coupling on the performance of adaptive arrays. *IEEE Transactions on Antennas and Propagation,* AP-31(5). Doi:10.1109/TAP.1983.1143128

Hamid, U., Wyne, S., and Butt, N.R., 2023. Joint model-order and robust doa estimation for underwater sensor arrays. *Sensors,* 23 (12), P. 5731. Doi:10.3390/s23125731.

Hefferon, J., 2017. *Linear Algebra.* 3rd ed. Vermont, USA.

Horn, R.A., and Johnson, C.R., 2013. *Matrix analysis.* 2nd ed. New York. Cambridge University Press.

Hui, H.T., 2004. A new definition of mutual impedance for application in dipole receiving antenna arrays. *IEEE Antennas and Wireless Propagation Letters,* 3, pp. 364-367. Doi:10.1109/LAWP.2004.841209

Hui, H.T., and Lu, S., 2006. *Receiving mutual impedance between two parallel dipole antennas*. IEEE Region 10 Conference, Hong Kong, China, pp. 1-4. Doi:10.1109/TENCON.2006.343692.

Islam, M.R., Chamok, N.H., and Ali, M., 2012. Switched parasitic dipole antenna array for high-data-rate body-worn wireless applications. *IEEE Antennas and Wireless Propagation Letters,* 11, pp. 693-696. Doi:10.1109/LAWP.2012.2204949.

Jasem, R.A., 2020. *High resolution direction of arrival estimation with switched active switched parasitic antenna arrays.* Perth, Australia: (Doctoral dissertation, Curtin University).

Jasem, R.A., 2023. Directive and steerable radiation pattern using SASPA Array. *Journal of Engineering,* 29(3), pp. 1–14. Doi:10.31026/j.eng.2023.03.01.

Jing, H., Wang, H., Liu, Z., and Shen, X., 2018. DOA estimation for underwater target by active detection on virtual time reversal using a uniform linear array. *Sensors,* 18(8), P. 2458, Doi:10.3390/s18082458.

Kausar, A., Mehrpouyan, H., Sellathurai, M., Qian, R., and Kausar, S., 2016. *Energy Efficient Switched Parasitic Array Antenna for 5G Networks and IoT*, Loughborough Antennas Propagation Conference (LAPAC). Doi:10.1109/LAPC.2016.7807569.

Lan, T., Huang, K., Jin, L., Xu, X., Sun, X., and Zhong, Z., 2022. DOA estimation algorithm for reconfigurable intelligent surface co-prime linear array based on multiple signal classification approach. *Information,* 13(2), P. 72. Doi:10.3390/info13020072.

Lui, H.-S., Hui, H.T., and Leong, M.S., 2009. A note on the mutual-coupling problems in transmitting and receiving antenna arrays. *IEEE Antennas and Propagation Magazine,* 51(5), pp. 171-176. Doi:10.1109/MAP.2009.5432083

Roy, R., and Kailath, T., 1989. ESPRIT – Estimation of signal parameters via rotational invariance techniques. *IEEE Transactions on Acoustics, Speech, and Signal Processing,* 37(7), pp. 984-995. Doi:10.1109/29.32276

Schmidt, R.O., 1986. Multiple emitter location and signal parameter estimation. *IEEE Transactions on Antennas and Propagation,* 34(3), pp. 276-280. Doi:10.1109/TAP.1986.1143830

Shaghaghi, M., and Vorobyov, S.A., 2015. Subspace leakage analysis and improved DOA estimation with small sample size. *IEEE Transactions on Signal Processing,* 63(12), pp. 3251-3265. Doi:10.1109/TSP.2015.2422675

Sun, C., and Yang, Y.X., 2004. On beampattern design for beamspace music. *Acoust. Sci., and Tech.,* 25(1), pp. 2-8. Doi:10.1250/ast.25.2.

Svantesson, T., and Wennstrom, M., 2001. *High-resolution direction finding using a switched parasitic antenna.* Singapore, in Proc. 11th IEEE Signal Processing Workshop on Statistical Signal Processing, pp. 508–511. Doi:10.1109/SSP.2001.955334

Thiel, D.V., and Smith, S., 2002. *Switched parasitic antennas for cellular communications.* Artech House.

Tuncer, E., and Friedlander, B., 2009. *Classical and modern direction-of-arrival estimation.* London, Academic Print.

Van Trees, H.L., 2002. *Optimal array processing theory. Part IV of Detection, Estimation, and Modulation Theory.* New York, John Wiley and Sons, Inc.

Wan, L., Han, G., Shu, L., Chan, S., and Zhu, T., 2016. The application of DOA estimation approach in patient tracking systems with high patient density. *IEEE Transactions on Industrial Informatics.,* 12, pp. 2353-2364. Doi:10.1109/TII.2016.2569416.

Yamada, H., Ogawa, Y., and Yamagucji, Y., 2005. *Mutual coupling compensation in array antenna for high-resolution DOA estimation.* Proceedings of ISAP2005, SEOUL, KOREA

Yu, Y., and Hui, H.T., 2011. Design of Mutual compensation network for a small receiving monopole array. *IEEE Transactions on Microwave Theory and Techniques,* 59(9), pp. 2241-2245. Doi: 10.1109/TMTT.2011.2160728

Zhang, R., Xu, K., Quan, Y., Zhu, S., and Xing, M., 2021. Signal Subspace Reconstruction for DOA detection using quantum-behaved particle swarm optimization. *Remote Sens.,* 13 (13), P. 2560. Doi:10.3390/rs13132560.

Zhao, T., Luo, C., Zhou, J., Guo, D., Chen, N., and Casaseca-de-la-Higuera, P., 2020. DoA prediction based beamforming with low training overhead for highly-mobile UAV communication with cellular networks. *Appl. Sci. ,* 10(13), P. 4420. Doi:10.3390/app101344.